
Towards Calibrated Robust Fine-Tuning of Vision-Language Models

Changdae Oh*
University of Seoul

Hyesu Lim*
KAIST

Mijoo Kim
Chung-Ang University

Dongyoon Han
NAVER AI Lab

Sangdoon Yun
NAVER AI Lab

Jaegul Choo
KAIST

Alexander Hauptmann
Carnegie Mellon University

Zhi-Qi Cheng⁺
Carnegie Mellon University

Kyungwoo Song⁺
Yonsei University

Abstract

Improving out-of-distribution (OOD) generalization through in-distribution (ID) adaptation is a primary goal of robust fine-tuning methods beyond the naive fine-tuning approach. However, despite decent OOD generalization performance from recent robust fine-tuning methods, OOD confidence calibration for reliable machine learning has not been fully addressed. This work proposes a robust fine-tuning method that improves both OOD accuracy and calibration error in Vision Language Models (VLMs). Firstly, we show that both types of errors have a shared upper bound consisting of two terms of ID data: 1) calibration error and 2) the smallest singular value of the input covariance matrix. Based on this insight, we design a novel framework that conducts fine-tuning with a constrained multimodal contrastive loss enforcing a larger smallest singular value, which is further aided by the self-distillation of a moving averaged model to achieve well-calibrated prediction. Starting from an empirical validation of our theoretical statements, we provide extensive experimental results on ImageNet distribution shift benchmarks that demonstrate the effectiveness of our method. Our code is available [here](#).

1 Introduction

Foundation models [5] have been extensively used to fine-tune downstream tasks using a pre-training-fine-tuning approach, employing generalized knowledge from large pre-training data to achieve both in-distribution (ID) and out-of-distribution (OOD) performance. After Wortsman et al. [53] and Kumar et al. [25] amplified the discussion on the robustness of recent Vision-Language Models (VLM)s [40, 22, 39] under distribution shifts, a wide range of research has followed [26, 13, 26, 49, 37] so-called *robust fine-tuning*.

Despite the advancements of the methods, we find that an important criterion for trustworthy machine learning (ML) has been overlooked – *confidence calibration* [33, 7] that quantifies how close the confidence of our predictor is to the actual correctness of predictions. As shown in Figure 1, existing robust fine-tuning methods hurt the confidence calibration in terms of expected calibration error (ECE) [34] on OOD data while they show improvements on OOD accuracy compared to the zero-shot performance. In this work, we introduce a calibrated robust fine-tuning method (**CaRot**) that simultaneously improves calibration and accuracy on OOD data.

*Equal contribution (changdae.oh@uos.ac.kr; hyesulim@kaist.ac.kr)

⁺Co-correspondence (zhiqic@cs.cmu.edu; kyungwoo.song@yonsei.ac.kr)

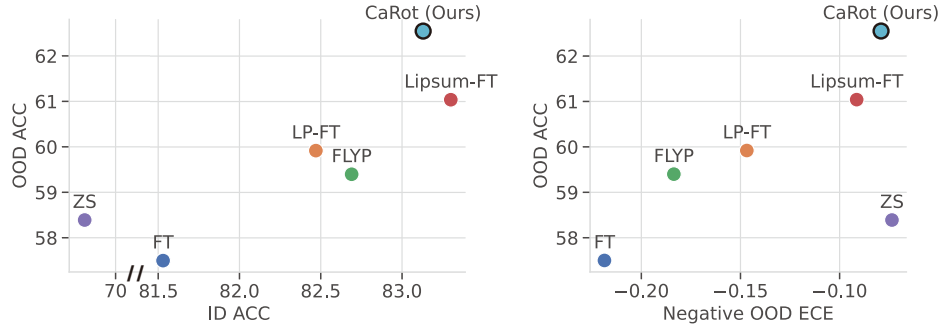


Figure 1: **OOD accuracy vs. ID accuracy (left) and negative OOD ECE (right)**. Notice that the competing methods – FLYP [13], LP-FT [25], and Lipsum-FT [36] – improve generalization over the zero-shot baseline (ZS) and naive fine-tuning (FT) but suffer from OOD miscalibration, presumably due to concerning model generalization solely at fine-tuning. Our CaRot outperforms existing methods on both OOD generalization and calibration by large margins. To maintain consistency in the plots, where desired values are shown on the right side of the x-axis, we report negative OOD ECE. ID ACC refers to ImageNet-1K top-1 accuracy; OOD ACC and ECE refer to the averaged accuracy and ECE of the five ImageNet distribution shifts (ImageNetV2, ImageNet-R, ImageNet-A, ImageNet-Sketch, and ObjectNet), respectively. Detailed numbers are reported in Table 2 and 3.

Confidence calibration is a key aspect of reliable machine learning, essential for avoiding high-confidence incorrect predictions in real-world decision-making systems. This is particularly crucial in high-stakes tasks like autonomous driving and healthcare applications. After a seminal work [14] revealed the miscalibration problem of high-performing neural networks, a plethora of attempts followed to improve the calibration of neural network models through post-hoc adjustments [56, 14, 24, 59, 15] or train-time regularizations [58, 45, 48, 32, 31]. However, many of them focus on improving calibration for ID samples, and methods for enhancing OOD calibration usually require OOD samples at train time [54, 12]. Moreover, these approaches commonly focus on calibration alone without ensuring improvement in other quantities, e.g., accuracy. In this work, we explore a unified framework that jointly considers calibration and accuracy (particularly on OOD data).

To accomplish low classification and calibration errors on OOD samples when only ID samples are available, we conduct theoretical analyses of those OOD errors. To be specific, we derive an upper bound that is shared with OOD classification error and OOD calibration error composed with two quantities on ID samples: 1) the reciprocal of the smallest singular value of the normalized covariance matrix of data representation and 2) the calibration error. Different from the existing bounds focusing on either one of classification or calibration error [4, 63, 54], we address both classification and calibration errors in a single unified bound. It is worth noting that we can compute the chief components of our bound without relying on unlabeled OOD samples [3].

Motivated by these theoretical analyses, we propose a new multimodal contrastive loss that promotes the smallest singular value of input image representation to become larger by enforcing the orthogonality of the final linear projection layer. Furthermore, to understand the proposal’s working mechanism in depth, we present an interpretation of our new multimodal contrastive loss as a process of seeking the low-rank approximation of cross-covariance matrix over image-text representations with reduced parameter space via orthogonality constraint. Meanwhile, to enhance confidence calibration on ID samples during fine-tuning, we utilize a self-distillation (SD) with an exponential moving average (EMA) teacher model. This EMA SD encourages a student model to learn semantic similarity structures of representations from teacher predictions across diverse contrastive pairs, appropriately adjusting confidence per each instance.

We first validate our new error bounds with synthetic datasets to show that the bounds hold empirically. Then, evaluate our method by conducting extensive experiments of fine-tuning CLIP [40] on ImageNet-1K [8] classification task under natural shift (ImageNet-V2/R/A/Sketch and ObjectNet). We demonstrate the effectiveness of our proposed framework for robust generalization and calibration by observing significant improvement in terms of expected calibration error and accuracy on ID/OOD datasets.

Contributions. 1) We point out that existing fine-tuning methods do not adequately achieve satisfactory OOD generalization and calibration simultaneously. 2) We provide theoretical analysis for classification and calibration errors on the OOD domain and show that they are both bounded from above by ID calibration error and the smallest singular value of the covariance matrix over ID input representation. 3) Based on our theoretical analyses, we devise a calibrated robust fine-tuning method, CaRot, that reduces the upper bound of OOD classification and calibration errors by conducting constrained multimodal contrastive learning with EMA self-distillation. 4) We first present empirical evidence for our theory on a synthetic dataset and demonstrate the efficacy of CaRot via extensive evaluations on ImageNet-1K distribution shifts in terms of accuracy and calibration error on ID and OOD domains.

2 Preliminary

Robust fine-tuning aims to achieve consistently high performance on both training (ID) and related but different test distributions (OOD). For validation, we commonly consider a covariate shift scenario for the classification task, where both ID and OOD domains share the class categories ($\mathcal{Y}_{\text{ID}} = \mathcal{Y}_{\text{OOD}}$) and have the same conditional distribution $P(Y|X)$, but have different marginal distributions over input X . That is, $P_{\text{ID}}(X) \neq P_{\text{OOD}}(X)$ but $P_{\text{ID}}(Y|X) = P_{\text{OOD}}(Y|X)$. Here, we evaluate the robustness of a model, which is fine-tuned on a training split of ID domain, on a test split of ID and that of OOD domains.

Confidence calibration is a concept of matching the softmax probabilities outputted for different inputs to the expected accuracy on these inputs. In a K -way classification setting, let $X \in \mathbb{R}^d$ and $Y \in \{1, \dots, K\}$ be random variables indicating inputs and labels, respectively. A dataset with N independent samples from the joint distribution $P(X, Y) = P(Y|X)P(X)$ is denoted by $\{(x_n, y_n)\}_{n=1}^N$. Let f be a classifier and $f(y|x) = \hat{p}$ be a confidence, i.e., the maximum of output probability corresponding to its prediction \hat{y} . We say a model is *perfectly-calibrated* when $\mathbb{P}(\hat{y} = y | \hat{p} = p) = p, \forall p \in [0, 1]$. To measure the calibration of a model, the model calibration can be derived as $\mathbb{E}[|\mathbb{P}(\hat{y} = y | \hat{p} = p) - p|]$. In practice, we use expected calibration error (ECE) [34] as an empirical approximation of the model calibration, which is a weighted average of bin-wise miscalibration. The ECE divides the confidence score of N samples into M uniform confidence bins $\{B_m\}_{m=1}^M$ and takes the mean of the gap between accuracy (acc) and confidence (conf) over the bins weighted by the number of samples in the bins, i.e., $\text{ECE} = \sum_{m=1}^M \frac{|B_m|}{N} |\text{acc}(B_m) - \text{conf}(B_m)|$.

3 Theoretical Analysis on OOD Generalization and Calibration

We first identify the factors that affect OOD generalization and calibration errors under circumstances where only ID data is accessible. We take inspiration from the generalization bound of domain adaptation literature [4, 63] while remarkably adapting the analysis to consider both OOD classification and calibration error at the same time in a more practical way.

Let \mathcal{D} be a domain on input space \mathcal{X} and $\mathcal{Y} = \{0, 1\}$ be a label space for a binary classification. Among the hypothesis function $h : \mathcal{X} \rightarrow [0, 1]$, we define $h_0(\cdot)$ as a desired calibrated predictor for label y , which minimizes the calibration error $\mathbb{E}_{x \sim \mathcal{D}}[(h(x) - c(x))^2]$ [33], where $c(x) = \mathbb{E}_y[y|h(x)]$ is the expected value of y given a prediction $h(x)$. That is, h_0 always produces the calibrated prediction for y given x so that the output confidence $h_0(x)$ matches the expectation of y over the subset of samples that have the same confidence as $h_0(x)$. Our goal is to learn a hypothesis function $h(\cdot)$ that outputs reliable probability on samples from the unseen OOD domain, which is defined by a distribution \mathcal{D}_{OOD} , as well as on the ID domain \mathcal{D}_{ID} , where the predictor is trained on. In essence, the error $\varepsilon_{\mathcal{D}}(h) = \mathbb{E}_{x \sim \mathcal{D}}[(h(x) - h_0(x))^2]$ should be small for two different domains $\mathcal{D} \in \{\mathcal{D}_{\text{ID}}, \mathcal{D}_{\text{OOD}}\}$. In this work, we concentrate on the covariate shift scenario (§2) that only the marginal distribution over \mathcal{X} changes while the distribution over \mathcal{Y} is preserved.

Let the optimal hypothesis h^* , which minimizes a combination of errors on both ID and OOD domain, be $h^* := \arg \min_{h \in \mathcal{H}} \varepsilon_{\mathcal{D}_{\text{ID}}}(h) + \varepsilon_{\mathcal{D}_{\text{OOD}}}(h)$, and Δ denote the optimal joint error $\Delta := \varepsilon_{\mathcal{D}_{\text{ID}}}(h^*) + \varepsilon_{\mathcal{D}_{\text{OOD}}}(h^*)$. We derive our novel bounds for the OOD calibration error and OOD classification error.

Theorem 3.1. *Let $h : \mathcal{X} \rightarrow [0, 1]$ be a real-valued function which has structure $h(x) = \sum_{i=1}^d h_i(x_i)$ where h_i is an arbitrary one-dimensional function, and $h(\cdot)$ is in a hypothesis class \mathcal{H} that has pseudo*

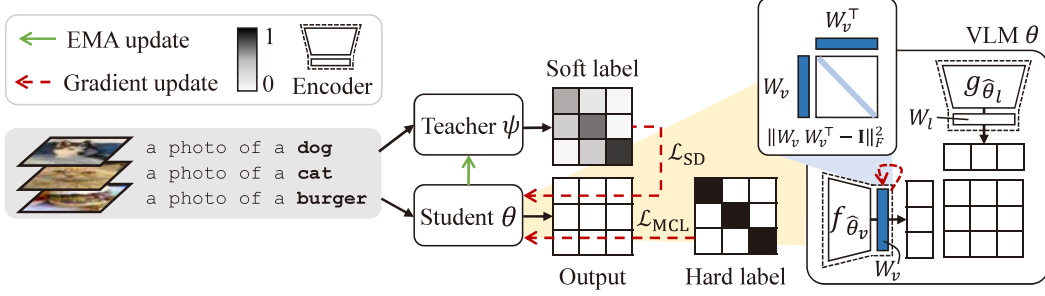


Figure 2: **Overview of CaRot.** We fine-tune VLM using a multimodal contrastive loss with an orthogonality constraint on visual projection layer (eq.(4)) and self-distillation \mathcal{L}_{SD} (eq.(5)) that takes predictions of EMA teacher ψ as soft target labels to update the student model θ . The darker and the lighter elements denote values closer to 1 and 0, respectively. Both teacher and student models share identical VLM architecture consisting of image $f_{\theta_v} := [f_{\hat{\theta}_v}; W_v]$ and text $g_{\theta_t} := [g_{\hat{\theta}_t}; W_t]$ encoders, where W is the last projection layer. Given (image, text) pair data, the model outputs the similarity map across image-text representations.

dimension $\mathcal{P}dim(\mathcal{H}) = d_h$, $\hat{\mathcal{D}}_{ID}$ be an N -size empirical distribution on ID domain. If (x_i, x_j) is a bi-variate Gaussian random variable for every $i, j \in [d]$, then for any $\delta \in (0, 1)$ and for all h , the following bounds hold with probability at least $1 - \delta$:

$$i) \varepsilon_{\mathcal{D}_{OOD}}(h) \leq \varepsilon_{\hat{\mathcal{D}}_{ID}}(h) + \frac{d}{\sigma_{\min}(\tilde{\Sigma}_{\mathcal{D}_{ID}})} + \Delta + \mathcal{O}\left(\sqrt{\frac{1}{N} \log\left(\frac{N}{d_h}\right)^{d_h} \left(\frac{1}{\delta}\right)}\right), \quad (1)$$

$$ii) \mathbb{E}_{\mathcal{D}_{OOD}}[(h(x) - y)^2] + \mathbb{E}_{\mathcal{D}_{OOD}}[c(x)^2] - 1 \leq \varepsilon_{\hat{\mathcal{D}}_{ID}}(h) + \frac{d}{\sigma_{\min}(\tilde{\Sigma}_{\mathcal{D}_{ID}})} + \Delta + \mathcal{O}\left(\sqrt{\frac{1}{N} \log\left(\frac{N}{d_h}\right)^{d_h} \left(\frac{1}{\delta}\right)}\right), \quad (2)$$

where $\tilde{\Sigma}_{\mathcal{D}_{ID}} := \mathbb{E}_{\mathcal{D}_{ID}}[\tilde{x}\tilde{x}^T]$ is a covariance matrix of d -dimensional normalized input $\tilde{x} = (\tilde{x}_1, \dots, \tilde{x}_d)$, where $\tilde{x}_i := (x_i - \mathbb{E}[x_i])\text{Var}(x_i)^{-1/2}$ and $\sigma_{\min}(M)$ is the smallest singular value of a matrix $M \in \mathbb{R}^{d_1 \times d_2}$. These theoretical results can be directly applied to the intermediate representation of a neural network by setting the input variable x as a representation vector [3, 64], so we will assume the input as an image representation of the visual encoder in following sections. Note that 1) the LHS of the first inequality (eq.(1)) indicates **OOD calibration error**, 2) two terms in the LHS of the second inequality (eq.(2)) denote **OOD classification error** in terms of L_2 loss and prediction sharpness in OOD domain, and 3) both inequalities have the same RHS, which contains the empirical estimate of **ID calibration error**, the reciprocal of the **smallest singular value of ID input covariance matrix**, and remaining irreducible terms that depend on the problem setup.

Based on our analysis, we expect the potential of reducing the upper bound of OOD calibration error and the sum of OOD classification error and prediction sharpness by minimizing the first two terms of RHS in both bounds: the empirical ID calibration error and the reciprocal of minimum singular value of the normalized ID covariance matrix. In §4, we devise a realization of this theoretical concept.

4 Method

Our goal is to achieve OOD generalization and calibration through ID adaptation of pre-trained VLMs. Motivated by our analysis in §3, we propose a calibrated robust fine-tuning method that enlarges the smallest singular value of the covariance matrix over ID input representation while improving ID calibration, thereby lowering the upper bound of OOD calibration and generalization error. Following previous works [53, 25, 13], we set CLIP [40] as our target VLM and focus the scope of validation to image classification task. An overview of our method is illustrated in Figure 2.

4.1 Robust fine-tuning with constrained multimodal contrastive learning

In order to adapt a pre-trained VLM on image classification tasks, the cross-entropy loss is the most common choice as an objective function. However, there are emerging shreds of evidence supporting

the use of contrastive loss (CL) for robust adaptation [61, 43, 13], especially when the model is pre-trained via CL. Witnessing its empirical success on OOD generalization [13], we leverage a CL-based learning strategy for VLM fine-tuning. CLIP consists of image encoder $f_{\theta_v}(\cdot) = f_{\hat{\theta}_v}(\cdot)W_v^T$ and text encoder $g_{\theta_l}(\cdot) = g_{\hat{\theta}_l}(\cdot)W_l^T$, where the encoders are composed with backbone models ($f_{\hat{\theta}_v}(\cdot), g_{\hat{\theta}_l}(\cdot)$) and projection layers (W_v^T, W_l^T). The encoders produce L_2 -normalized representations to compute the similarity between image and text inputs. Given N pairs of (image, text) $\{(I_i, T_i)\}_{i=1}^N$, a common form of multimodal contrastive loss (MCL) can be written as

$$\begin{aligned} \mathcal{L}_{\text{MCL}}(\theta) &:= \frac{1}{2N} \sum_{i=1}^N -\log \frac{\exp(f_{\theta_v}(I_i) \cdot g_{\theta_l}(T_i))}{\sum_{j=1}^N \exp(f_{\theta_v}(I_i) \cdot g_{\theta_l}(T_j))} \\ &+ \frac{1}{2N} \sum_{i=1}^N -\log \frac{\exp(f_{\theta_v}(I_i) \cdot g_{\theta_l}(T_i))}{\sum_{j=1}^N \exp(f_{\theta_v}(I_j) \cdot g_{\theta_l}(T_i))} + R(\theta_v, \theta_l), \end{aligned} \quad (3)$$

where $\theta = \{\theta_v, \theta_l\}$ are the parameters of image and text encoders and $R(\theta_v, \theta_l)$ reflects general regularization strategies in CL [6, 17]. We update both image and text encoders during fine-tuning as done in the pre-train phase and use OpenAI templates [40] to create (image, text) pairs from a downstream classification dataset that consists of (image, class) pairs.

Meanwhile, the basic form of \mathcal{L}_{MCL} does not inform anything about the singular value distribution of learned representation. In §3, we showed that the reciprocal of the smallest singular value constitutes the shared upper bound, i.e., the larger the smallest singular value is, the lower the upper bound becomes. To encourage this, we put a soft constraint term to \mathcal{L}_{MCL} that enforces the final projection matrix W_v of the visual encoder to be orthogonal and hence the output image representation matrix to have a large effective rank, as in below:

$$\mathcal{L}_{\text{MCL-con}}(\theta) := \mathcal{L}_{\text{MCL}}(\theta) + \lambda_{\text{OC}} \mathcal{L}_{\text{OC}}(W_v), \quad \mathcal{L}_{\text{OC}}(W_v) = \|W_v W_v^T - \mathbf{I}\|_F^2, \quad (4)$$

where \mathbf{I} is an identity matrix that has the same shape with W_v and λ_{OC} is a strength of the orthogonality constraint¹. While recklessly increasing the singular values might hinder ID adaptation, our orthogonal constraint mitigates the degradation of performance by pursuing not only the smallest singular values to be large but also the largest singular values to be small which is important for generalization on ID data [60]. Interestingly, this contrastive loss with regularization terms can be viewed as a singular value decomposition (SVD) on the cross-covariance matrix of image-text representations with an orthogonality constraint.

To be specific, by following Nakada et al. [35], under a linear representation assumption, a gradient descent step of $\mathcal{L}_{\text{MCL-con}}$ boils down to the maximization of the SVD objective, which aims to find a low-rank approximation of the normalized cross-covariance matrix $S(\beta)$ ² as follow:

$$\begin{aligned} \arg \min_{W_v, W_l} \mathcal{L}_{\text{MCL-con}}(W) &:= \frac{1}{N} \sum_{i=1}^N -\log \frac{\exp(W_v \hat{I}_i \cdot W_l \hat{T}_i)}{\sum_{j=1}^N \exp(W_v \hat{I}_i \cdot W_l \hat{T}_j)} \\ &+ \frac{1}{N} \sum_{i=1}^N -\log \frac{\exp(W_v \hat{I}_i \cdot W_l \hat{T}_i)}{\sum_{j=1}^N \exp(W_v \hat{I}_j \cdot W_l \hat{T}_i)} + R(W_v, W_l) + \lambda_{\text{OC}} \|W_v W_v^T - \mathbf{I}\|_F^2 \\ &\approx \arg \max_{W_v, W_l} \text{SVD}(S(\beta)) := \text{tr}(W_v S(\beta) W_l^T) - (\rho/2) \|W_v^T W_l\|_F^2 \quad \text{subject to } \|W_v W_v^T - \mathbf{I}\|_F^2 = 0, \end{aligned}$$

where we adopt $R(W_v, W_l) = (\rho/2) \|W_v^T W_l\|_F^2$ for $\rho > 0$ as a regularization term to promote the encoders to capture diverse features as in Ji et al. [21]. Here, we assume that the input of $\mathcal{L}_{\text{MCL-con}}$ is the penultimate representation of VLM’s encoders, i.e., $(\hat{I}_i, \hat{T}_i) = (f_{\hat{\theta}_v}(I_i), g_{\hat{\theta}_l}(T_i))$, and $W = \{W_v, W_l\}$ is a set of projection matrices (i.e., last layers of each encoder). This equivalence between \mathcal{L}_{MCL} and SVD allows us to understand the working mechanism of our proposed objective. That is, minimizing $\mathcal{L}_{\text{MCL-con}}$ can be interpreted as finding a good approximation over the cross-modal covariance matrix by seeking the direction of maximal variation among image-text representations,

¹While it is also possible to inject constraint on the text projection matrix W_l , we only do it for W_v because our concern is about the singular value of image representations for downstream tasks. We observed degradations of accuracy (ID: -0.01, OOD: -0.15) and ECE (ID: -0.002, OOD: -0.02) by adding the constraint on W_v .

² $S(\beta) := \frac{1}{N} \sum_{i=1}^N \beta_i \hat{I}_i \hat{T}_i^T - \frac{1}{N} \sum_{i \neq j} \beta_{ij} \hat{I}_i \hat{T}_j^T$, where β_i and β_{ij} depend the choice of non-linear function over dot product between image and text representations.

while enforcing a large smallest singular value of the covariance matrix of image representation via orthogonality constraint on W_v . In §5, we validate that $\mathcal{L}_{\text{MCL-con}}$ significantly increases the smallest singular values and results in better OOD generalization and calibration on downstream tasks.

4.2 Calibration during robust fine-tuning

In the previous section, we devise a new multimodal contrastive loss that promotes large $\sigma_{\min}(\tilde{\Sigma}_{\mathcal{D}_{\text{ID}}})$. We now address the next component standing for ID calibration, which is another crucial component according to our theoretical analysis. While there are numerous approaches to enhance calibration during neural network training [32, 48, 45, 1], we notice the promising results of knowledge distillation-based calibration approaches [55, 62]. These approaches encourage the model to learn from input-dependent smoothed labels that effectively mitigate the overconfidence issue, which is commonly associated with miscalibration. We employ a self-distillation (SD) method for ID calibration in that distilling supervision would help avoid overconfidence.

Specifically, we first initialize both teacher and student networks with a pre-trained CLIP model (including both image and text encoders); update the student model using gradient descent for every iteration while slowly updating the teacher model that has $\psi = \{\psi_v, \psi_l\}$ as parameters using EMA with the momentum of α at every $t > 1$ iteration, i.e., $\psi \leftarrow \alpha\psi + (1 - \alpha)\theta$. Rather than hosting another VLM or pre-trained CLIP as a teacher model, we adopt a self-evolving EMA network as a teacher, in accordance with the notable observation of the impressive robustness of weight-space ensembling among identical structure networks [53, 41]. With the EMA teacher ψ and the learning student θ , we construct a self-distillation loss term for N data pairs as:

$$\mathcal{L}_{\text{SD}}(\theta) := \sum_{i=1}^N [KL(\tilde{q}_i^I || q_i^I) + KL(\tilde{q}_i^T || q_i^T)], \quad (5)$$

where KL denotes Kullback–Leibler divergence, $q_i^I = \text{softmax}(\{f_{\theta_v}(I_i) \cdot g_{\theta_l}(T_j)\}_{j=1}^N)$ and $q_i^T = \text{softmax}(\{f_{\theta_v}(I_j) \cdot g_{\theta_l}(T_i)\}_{j=1}^N)$ are student outputs, and \tilde{q}_j^I and \tilde{q}_j^T are teacher outputs which are similarly defined by replacing the student parameter θ with teacher ψ . Presumably, label smoothing (LS) [47] achieves effects similar to what we intended, but we argue that LS would have overconfidence issues, as demonstrated in the Appendix §B.

We complete the learning objective as a summation of $\mathcal{L}_{\text{MCL-con}}$ and \mathcal{L}_{SD} with a coefficient λ_{SD} , i.e., $\mathcal{L} = \mathcal{L}_{\text{MCL}} + \lambda_{\text{OC}}\mathcal{L}_{\text{OC}} + \lambda_{\text{SD}}\mathcal{L}_{\text{SD}}$. The novel combination of these two components contributes to ensuring a larger smallest singular value of image representation and ID calibration simultaneously, which induces calibrated robust fine-tuning (**CaRot**) on diverse distribution shifts.

5 Experiments

In § 5.1, we first show empirical evidence of the error bounds that we derived in §3. We then provide experimental setup (§5.2) and discuss the empirical analyses on benchmark datasets (§5.3).

5.1 Numerical analysis on error bounds

Our theoretical analysis in §3 revealed the capability of managing OOD classification and calibration errors using the same quantities over ID domain at the same time. Before conducting real-world evaluations, we verify our theoretical analysis with our toy experiments that simulate distribution shifts. To be specific, we generate a binary classification dataset with 1000-dimensional Gaussian features where the mean of features are partly shifted across different test environments (ID, OOD). We train a three-layer network with regularization terms: Born-Again-Network (BAN)-style self-distillation [10] for calibration (\mathcal{L}_{SD}) and the orthogonality constraint (shown in eq.(4)) for the singular value (\mathcal{L}_{OC}). Detailed descriptions of the experimental setup are provided in Appendix §A.1.

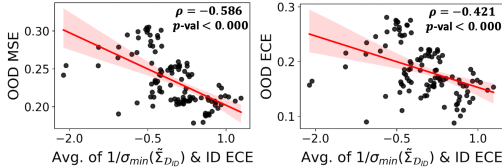


Figure 3: **Analysis of error bounds on synthetic data.** Plots on the left side show RHS (x-axis) and LHS (y-axis; MSE for eq.(2) and ECE for eq.(1)) of the inequalities in §3. We denote MSE for the mean squared error, \mathcal{L}_{OC} for the singular value regularization, and \mathcal{L}_{SD} for the calibration regularization.

Figure 3 visualizes the results of Pearson correlation analysis between the average of $1/\sigma_{min}(\tilde{\Sigma}_{D_{ID}})$ and ECE from ID samples and OOD MSE/ECE over 111 trained models. Here, we observe strong correlations between the average of $1/\sigma_{min}(\tilde{\Sigma}_{D_{ID}})$ and ID ECE (x-axis), and OOD classification and calibration errors (y-axis). Additional results on the best models per each regularization term are showcased on the Table 1, which also indicates that reducing the upper bound results in better OOD generalization and calibration. These analyses demonstrate our upper bound eq.(3) empirically holds.

5.2 Evaluation on distribution shift benchmarks

Training and evaluation. We adopt CLIP ViT-B/16 as our VLM backbone and evaluate each fine-tuning method, including CaRot, in terms of calibration (with ECE) and accuracy under distribution shifts. For downstream tasks, we consider the ImageNet-1K (IN) classification and regard it as our ID domain. For all methods, we optimize the model parameters using the AdamW with a batch size of 512 over 10 epochs. Fine-tuned models are evaluated under varying distribution shifts.

Benchmark datasets. We consider IN-V2 [42], IN-R [18], IN-A [19], IN-S [52], and ObjectNet [2]. We refer to these five datasets as OOD throughout the following sections unless it is specified as a different dataset.

Baseline methods. We benchmark CaRot alongside zero-shot inference (ZS) and fine-tuning methods: standard fine-tuning (FT), LP-FT [25], FLYP [13], and Lipsum-FT [36]. Refer §A for further details of each method. In Appendix Table A, B, and C, we compare results when applying post-hoc

Table 1: The best case values of two terms of RHS (ID σ_{min} and ID ECE) and LHS – OOD errors (MSE and ECE) in the bounds of Theorem 3. Reported values are an average of three repeated runs.

Method	ID		OOD	
	σ_{min} (\uparrow)	ECE (\downarrow)	MSE (\downarrow)	ECE (\downarrow)
Baseline	2.0887	0.1666	0.2581	0.2477
\mathcal{L}_{OC}	<u>4.9630</u>	0.1528	<u>0.1932</u>	0.1781
\mathcal{L}_{SD}	3.1354	<u>0.1308</u>	0.2170	<u>0.1720</u>
$\mathcal{L}_{OC}, \mathcal{L}_{SD}$	<u>6.5961</u>	<u>0.1391</u>	<u>0.1877</u>	<u>0.1596</u>

Table 2: **ImageNet accuracy.** We report the accuracy on ImageNet and its distribution shift variants by fine-tuning CLIP ViT-B/16 with five methods. The best and the second-best in each column are underlined.

Method	IN \uparrow	IN-V2 \uparrow	IN-R \uparrow	IN-A \uparrow	IN-S \uparrow	ObjectNet \uparrow	Avg. shifts \uparrow
ZS	68.33	61.93	<u>77.71</u>	<u>49.95</u>	48.26	54.17	58.39
FT	81.53	71.66	70.14	44.01	49.11	52.56	57.50
LP-FT	82.47	72.71	72.84	49.31	50.28	54.45	59.92
FLYP	82.69	72.73	71.35	48.52	49.84	<u>54.86</u>	59.40
Lipsum-FT	<u>83.30</u>	<u>73.60</u>	75.90	49.90	<u>51.40</u>	54.38	<u>61.04</u>
CaRot (Ours)	83.13	<u>74.11</u>	<u>77.71</u>	<u>51.60</u>	<u>52.71</u>	<u>56.60</u>	<u>62.55</u>

Table 3: **ImageNet ECE.** Along with Table 2, we report the ECE on ImageNet and its distribution shifts to compare with other fine-tuning methods, which demonstrates our out-of-distribution (OOD) calibration performance. The best and the second-best in each column are underlined (See Figure B for details).

Method	IN \downarrow	IN-V2 \downarrow	IN-R \downarrow	IN-A \downarrow	IN-S \downarrow	ObjectNet \downarrow	Avg. shifts \downarrow
ZS	0.0570	0.0548	<u>0.0541</u>	<u>0.0967</u>	<u>0.0850</u>	<u>0.0780</u>	<u>0.0736</u>
FT	0.0884	0.1468	0.1164	0.3000	0.2544	0.2753	0.2186
LP-FT	0.0505	0.0894	0.0613	0.2051	0.1659	0.2124	0.1468
FLYP	0.0635	0.1171	0.0967	0.2435	0.2200	0.2383	0.1836
Lipsum-FT	<u>0.0384</u>	<u>0.0516</u>	<u>0.0426</u>	0.1290	0.1023	0.1315	0.0914
CaRot (Ours)	<u>0.0470</u>	<u>0.0367</u>	0.0575	<u>0.1240</u>	<u>0.0699</u>	0.1075	<u>0.0791</u>

Table 4: **Ablation study on CaRot components.** We report accuracy and ECE on ImageNet (ID) and its distribution shifts (OOD). OOD values are averaged over five shifts. Values in brackets indicate the performance difference compared to the first row of each sub-table, and the **dark green** highlights the positive improvement.

\mathcal{L}_{MCL}	\mathcal{L}_{OC}	\mathcal{L}_{SD}	ID Acc.↑	ID ECE↓	OOD Acc.↑	OOD ECE↓
-	-	-	81.53	0.0884	57.50	0.2186
-	✓	-	81.45 (-0.08)	0.0874 (-0.0010)	59.10 (+1.60)	0.2051 (-0.0135)
-	-	✓	82.18 (+0.65)	0.0601 (-0.0283)	60.73 (+3.23)	0.1698 (-0.0488)
-	✓	✓	82.20 (+0.67)	0.0634 (-0.0250)	60.11 (+2.61)	0.1762 (-0.0424)
✓	-	-	82.69	0.0635	59.40	0.1836
✓	✓	-	82.51 (-0.18)	0.0651 (+0.0016)	59.51 (+0.11)	0.1803 (-0.0033)
✓	-	✓	83.03 (+0.34)	0.0523 (-0.0112)	62.28 (+2.88)	0.0772 (-0.1064)
✓	✓	✓	83.13 (+0.44)	0.0470 (-0.0165)	62.55 (+3.15)	0.0791 (-0.1045)

Table 5: **Analysis on coefficient terms of CaRot objective.** Along with Table 4, we report fine-grained analysis results on each term. We set λ_{OC} as 0.2 and λ_{SD} as 1.5 when ablating each other and for all experiments throughout the paper. We select the final values of λ_{OC} and λ_{SD} based on ID ECE and $\sigma_{\min}(\sum_{\mathcal{D}_{\text{ID}}})$, respectively.

λ_{OC}	ID		OOD		λ_{SD}	ID		OOD	
	Acc.↑	ECE↓	Acc.↑	ECE↓		Acc.↑	ECE↓	Acc.↑	ECE↓
0.0	83.03	0.0523	62.28	0.0772	0.0	82.51	0.0651	59.51	0.1803
0.1	83.18	0.0511	62.42	0.0779	0.5	83.07	0.0482	61.38	0.1377
0.2	83.13	0.0470	62.55	0.0791	1.0	83.23	0.0388	62.21	0.0997
0.5	83.04	0.0478	62.44	0.0798	1.5	83.13	0.0470	62.55	0.0791
1.0	83.09	0.0499	62.49	0.0781	2.0	82.72	0.0634	62.54	0.0781

techniques for robust fine-tuning (weight ensembling; WiSE-FT [53]) and post-hoc calibration (temperature scaling; TS [14]) methods.

Evaluation results. Table 2 and 3 highlight our argument that CaRot significantly enhances both generalization and calibration on OOD data. Under distribution shifts from IN to -V2, -R, -A, -S, and ObjectNet, CaRot favorably compares with the existing best fine-tuning methods by margin of 1.51 and 0.0123 for OOD top-1 accuracy and ECE, respectively, averaged over five shifted datasets. The reliability diagrams are provided in Appendix Figure B. We report the results with different VLM backbones, RN50 and ViT-L/14, in Table 7 (See Table G and H for details). CaRot consistently outperforms the baseline methods for these backbones, too. Furthermore, in Table 6, we provide additional comparisons with CAR-FT [28], Model Stock [20] and ARF [16].³

5.3 Empirical studies

Ablation study. In Table 4, we provide ablation study results to show the impacts of each component of CaRot. In line with our hypothesis, the results confirm that all three components boost OOD accuracy and calibration performance. The comparison of adopting and not adopting \mathcal{L}_{MCL} (we followed the naive fine-tuning approach for the latter) ascertains that employing contrastive loss as a fine-tuning objective is superior to cross-entropy loss for ID/OOD accuracy, consistent with the previous observations [13], and even extends to improvements in calibration as well. The ablations of the orthogonality constraint and adopting self-distillation validate our rationale behind adding the terms to our learning objective, where we expect them to lower the upper bound of OOD classification and calibration errors. Together, constraining the singular values of image representation on MCL and distilling EMA teacher’s predictions show the best results which aligned with results from the demonstration of error bounds in Fig 3. We further analyze the impact of each component by varying the strength coefficients in Table 5. We observe that the increased intensity of constraint improves ID and OOD performance to some degree, but there is a slight decline when the intensity is too strong. Meanwhile, the strength of self-distillation positively correlated with OOD accuracy and ECE, but there is a negative correlation between ID accuracy and ECE, which reflects the inevitable trade-off between ID adaptation and OOD generalization (Table F and E in Appendix provide further details).

³We report the averaged accuracy over four shifted datasets in this Table 6. Results for methods marked with an asterisk (*) are referenced from the respective original papers. The ECE results are not included due to the missing evaluations from the original papers.

Table 7: **ImageNet accuracy and ECE results on different backbones.** We provide summarized results on CLIP RN50 and ViT-L/14. The best and the second-best in each column are underlined. (See Table G and H for details.)

	Method	ID		OOD			ID		OOD		
		Acc.↑	ECE↓	Acc.↑	ECE↓		Acc.↑	ECE↓	Acc.↑	ECE↓	
RN50	ZS	59.83	0.0624	42.52	<u>0.0955</u>		ViT-L/14	75.55	<u>0.0590</u>	70.93	<u>0.0711</u>
	FT	<u>76.21</u>	0.0983	41.97	0.2804		85.26	0.0993	65.98	0.2036	
	LP-FT	<u>76.25</u>	0.1042	41.62	0.3274		84.74	0.1056	64.11	0.2521	
	FLYP	76.16	<u>0.0516</u>	<u>42.70</u>	0.2127		86.19	0.0729	<u>71.44</u>	0.1470	
	CaRot (Ours)	76.12	<u>0.0471</u>	<u>42.71</u>	<u>0.1714</u>		<u>86.95</u>	<u>0.0349</u>	<u>74.13</u>	<u>0.0737</u>	

Table 6: **ImageNet Acc. (except ObjectNet) with additional baselines.**

Method	IN↑	IN-V2↑	IN-R↑	IN-A↑	IN-S↑	Avg. shifts↑
ZS	68.33	61.93	77.71	49.95	48.26	59.46
FT	81.53	71.66	70.14	44.01	49.11	58.73
LP-FT	82.17	72.06	70.47	46.29	48.68	59.38
CAR-FT*	83.30	74.00	75.40	49.50	53.00	62.98
FLYP	82.69	72.73	71.35	48.52	49.84	60.61
Lipsum-FT	83.30	73.60	75.90	49.90	51.40	62.70
Model Stock*	84.10	74.80	71.80	51.20	51.80	62.40
ARF*	82.70	72.80	75.60	50.30	51.80	62.63
CaRot (Ours)	83.13	74.11	77.71	51.60	52.71	64.03

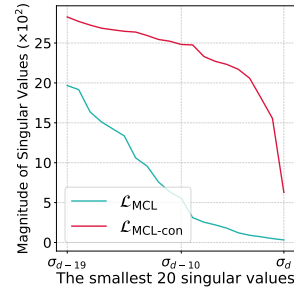


Figure 4: **Impact of $\mathcal{L}_{\text{MCL-con}}$**

Analysis on singular values. Figure 4 illustrates the last 20 singular values of the covariance matrix $\bar{I}^T \bar{I}$ where \bar{I} is a standardized image representations over N examples. Our proposed constrained contrastive loss $\mathcal{L}_{\text{MCL-con}}$ enlarges the small singular values compared to the conventional contrastive loss \mathcal{L}_{MCL} . This result verifies that adding the orthogonality constraint successfully reduces $1/\sigma_{\min}(\bar{\Sigma}_{\mathcal{D}_{\text{ID}}})$, the component of the shared upper bound we derived in §3, following our intention.

6 Related Work

Robust fine-tuning for visual foundation models. Beyond the ID generalization, there are a lot of works aiming at improving the generalization of fine-tuned models on the OOD domain. Some of them leverage the strong robustness of pre-trained model through weight-average [53, 20, 46] or regularization [46, 49, 50, 36] whereas others attribute to the robustness during fine-tuning from different part of model backbone [25, 26]. Besides, Goyal et al. [13] claim that aligning the learning objective during pre-training and fine-tuning is crucial for retaining the remarkable OOD generalization capability of the pre-trained model. Although the above methods have provided insights into the extrapolation of foundation models, confidence calibration has been unaddressed, which is crucial for reliable ML applications. We investigate the calibration of fine-tuned CLIP and propose a unified fine-tuning strategy that has theoretical support to achieve superior ID and OOD calibration alongside OOD generalization for the first time.

Confidence calibration. After some early research on calibrated prediction [33, 7], lots of follow-up studies have been conducted. As a seminal work, Guo et al. [14] revealed the miscalibration problem of neural networks, then, Minderer et al. [29] and LeVine et al. [27] provided a comprehensive analysis on the calibration of modern vision models with consideration on distribution shift. To improve the calibration of predictive models, Temperature Scaling (TS) [14] and Label Smoothing (LS) [47] are two representative methods in practice. TS-based approaches learn a temperature parameter itself [14, 12] or model [54, 23] to estimate the temperature to adjust the output probability of models, whereas LS-based methods focus on producing soft labels to mitigating overconfidence issues by a fixed [47, 32], randomized [48], or model-based [62, 57] smoothing strategies. However, existing approaches do not consider distribution shift [62], assume accessibility to target domain [12, 54], assume specific type of distribution shift [51], cannot adjust confidences individually [14, 47]. In this work, we adopt EMA self-distillation as an effective input-dependent calibration method and

show that the superior calibration results on in-domain samples can be transferred to other domains (without data from those domains) by pursuing the larger smallest singular value together.

7 Conclusion

While there have been numerous research endeavors to improve reliability during the model adaptation in the wilds, almost all of them meet the desired criteria only in half: OOD generalization or confidence calibration. This work attempts to address both OOD generalization and OOD calibration in a single framework. We first derive a shared upper bound for OOD classification and calibration errors which is constructed with the ID calibration error and the smallest singular value of ID input representation. We then devise a novel fine-tuning method CaRot, which promotes a larger smallest singular value and calibrated prediction through constrained multimodal contrastive loss and self-distillation. Our theoretical statements and proposed method are empirically validated through extensive experiments.

Limitation and Societal impact. Our research reached the scale of ViT-L. Due to resource constraints, we were unable to perform more experiments on larger models like ViT-G or ViT-H.

Societal impact. Our experiments utilize the ImageNet dataset, which is known for certain inherent biases, such as geographic or cultural biases. While our method achieves good generalization and calibration results that can positively impact numerous real-world applications, biases learned from the dataset could have negative downstream impacts.

References

- [1] Arsenii Ashukha, Alexander Lyzhov, Dmitry Molchanov, and Dmitry Vetrov. Pitfalls of in-domain uncertainty estimation and ensembling in deep learning. *arXiv preprint arXiv:2002.06470*, 2020.
- [2] Andrei Barbu, David Mayo, Julian Alverio, William Luo, Christopher Wang, Dan Gutfreund, Josh Tenenbaum, and Boris Katz. Objectnet: A large-scale bias-controlled dataset for pushing the limits of object recognition models. In *Advances in Neural Information Processing Systems (NeurIPS)*, 2019.
- [3] Shai Ben-David, John Blitzer, Koby Crammer, and Fernando Pereira. Analysis of representations for domain adaptation. In B. Schölkopf, J. Platt, and T. Hoffman, editors, *Advances in Neural Information Processing Systems*, volume 19. MIT Press, 2006. URL https://proceedings.neurips.cc/paper_files/paper/2006/file/b1b0432ceafb0ce714426e9114852ac7-Paper.pdf.
- [4] Shai Ben-David, John Blitzer, Koby Crammer, Alex Kulesza, Fernando Pereira, and Jennifer Vaughan. A theory of learning from different domains. *Machine Learning*, 79:151–175, 05 2010. doi: 10.1007/s10994-009-5152-4.
- [5] Rishi Bommasani, Drew A Hudson, Ehsan Adeli, Russ Altman, Simran Arora, Sydney von Arx, Michael S Bernstein, Jeannette Bohg, Antoine Bosselut, Emma Brunskill, et al. On the opportunities and risks of foundation models. *arXiv preprint arXiv:2108.07258*, 2021.
- [6] Ting Chen, Simon Kornblith, Mohammad Norouzi, and Geoffrey Hinton. A simple framework for contrastive learning of visual representations. In Hal Daumé III and Aarti Singh, editors, *Proceedings of the 37th International Conference on Machine Learning*, volume 119 of *Proceedings of Machine Learning Research*, pages 1597–1607. PMLR, 13–18 Jul 2020.
- [7] Morris H. DeGroot and Stephen E. Fienberg. The comparison and evaluation of forecasters. *Journal of the Royal Statistical Society. Series D (The Statistician)*, 1983. ISSN 00390526, 14679884.
- [8] Jia Deng, Wei Dong, Richard Socher, Li-Jia Li, Kai Li, and Li Fei-Fei. Imagenet: A large-scale hierarchical image database. In *IEEE Conference on Computer Vision and Pattern Recognition (CVPR)*, 2009.
- [9] Kefan Dong and Tengyu Ma. First steps toward understanding the extrapolation of nonlinear models to unseen domains. In *NeurIPS 2022 Workshop on Distribution Shifts: Connecting Methods and Applications*, 2022.
- [10] Tommaso Furlanello, Zachary Lipton, Michael Tschannen, Laurent Itti, and Anima Anandkumar. Born again neural networks. In *International conference on machine learning*, pages 1607–1616. PMLR, 2018.
- [11] Yaroslav Ganin, Evgeniya Ustinova, Hana Ajakan, Pascal Germain, Hugo Larochelle, François Laviolette, Mario March, and Victor Lempitsky. Domain-adversarial training of neural networks. *Journal of machine learning research*, 17(59):1–35, 2016.

- [12] Yunye Gong, Xiao Lin, Yi Yao, Thomas G Dietterich, Ajay Divakaran, and Melinda Gervasio. Confidence calibration for domain generalization under covariate shift. In *IEEE Conference on Computer Vision and Pattern Recognition (CVPR)*, 2021.
- [13] Sachin Goyal, Ananya Kumar, Sankalp Garg, Zico Kolter, and Aditi Raghunathan. Finetune like you pretrain: Improved finetuning of zero-shot vision models. In *IEEE Conference on Computer Vision and Pattern Recognition (CVPR)*, 2023.
- [14] Chuan Guo, Geoff Pleiss, Yu Sun, and Kilian Q Weinberger. On calibration of modern neural networks. In *International Conference on Machine Learning (ICML)*, 2017.
- [15] Kartik Gupta, Amir Rahimi, Thalaiyasingam Ajanthan, Thomas Mensink, Cristian Sminchisescu, and Richard Hartley. Calibration of neural networks using splines. *arXiv preprint arXiv:2006.12800*, 2020.
- [16] Jinwei Han, Zhiwen Lin, Zhongyisun Sun, Yingguo Gao, Ke Yan, Shouhong Ding, Yuan Gao, and Gui-Song Xia. Anchor-based robust finetuning of vision-language models. *arXiv preprint arXiv:2404.06244*, 2024.
- [17] Kaiming He, Haoqi Fan, Yuxin Wu, Saining Xie, and Ross Girshick. Momentum contrast for unsupervised visual representation learning. In *Proceedings of the IEEE/CVF Conference on Computer Vision and Pattern Recognition (CVPR)*, June 2020.
- [18] Dan Hendrycks, Steven Basart, Norman Mu, Saurav Kadavath, Frank Wang, Evan Dorundo, Rahul Desai, Tyler Zhu, Samyak Parajuli, Mike Guo, et al. The many faces of robustness: A critical analysis of out-of-distribution generalization. In *IEEE Conference on Computer Vision and Pattern Recognition (CVPR)*, 2021.
- [19] Dan Hendrycks, Kevin Zhao, Steven Basart, Jacob Steinhardt, and Dawn Song. Natural adversarial examples. In *IEEE Conference on Computer Vision and Pattern Recognition (CVPR)*, 2021.
- [20] Dong-Hwan Jang, Sangdoon Yun, and Dongyoon Han. Model stock: All we need is just a few fine-tuned models. *arXiv preprint arXiv:2403.19522*, 2024.
- [21] Wenlong Ji, Zhun Deng, Ryumei Nakada, James Zou, and Linjun Zhang. The power of contrast for feature learning: A theoretical analysis. *Journal of Machine Learning Research*, 24(330):1–78, 2023.
- [22] Chao Jia, Yinfei Yang, Ye Xia, Yi-Ting Chen, Zarana Parekh, Hieu Pham, Quoc Le, Yun-Hsuan Sung, Zhen Li, and Tom Duerig. Scaling up visual and vision-language representation learning with noisy text supervision. In *International conference on machine learning*, pages 4904–4916. PMLR, 2021.
- [23] Tom Joy, Francesco Pinto, Ser-Nam Lim, Philip HS Torr, and Puneet K Dokania. Sample-dependent adaptive temperature scaling for improved calibration. In *AAAI Conference on Artificial Intelligence (AAAI)*, 2023.
- [24] Meelis Kull, Miquel Perello Nieto, Markus Kängsepp, Telmo Silva Filho, Hao Song, and Peter Flach. Beyond temperature scaling: Obtaining well-calibrated multi-class probabilities with dirichlet calibration. *Advances in Neural Information Processing Systems (NeurIPS)*, 2019.
- [25] Ananya Kumar, Aditi Raghunathan, Robbie Jones, Tengyu Ma, and Percy Liang. Fine-tuning can distort pretrained features and underperform out-of-distribution. In *International Conference on Learning Representations (ICLR)*, 2022.
- [26] Yoonho Lee, Annie S Chen, Fahim Tajwar, Ananya Kumar, Huaxiu Yao, Percy Liang, and Chelsea Finn. Surgical fine-tuning improves adaptation to distribution shifts. In *International Conference on Learning Representations (ICLR)*, 2023.
- [27] Will LeVine, Benjamin Pikus, Pranav Raj, and Fernando Amat Gil. Enabling calibration in the zero-shot inference of large vision-language models. *arXiv preprint arXiv:2303.12748*, 2023.
- [28] Xiaofeng Mao, Yufeng Chen, Xiaojun Jia, Rong Zhang, Hui Xue, and Zhao Li. Context-aware robust fine-tuning. *International Journal of Computer Vision (IJCV)*, 132(5):1685–1700, 2024.
- [29] Matthias Minderer, Josip Djolonga, Rob Romijnders, Frances Hubis, Xiaohua Zhai, Neil Houlsby, Dustin Tran, and Mario Lucic. Revisiting the calibration of modern neural networks. *Advances in Neural Information Processing Systems (NeurIPS)*, 34, 2021.
- [30] Mehryar Mohri, Afshin Rostamizadeh, and Ameet Talwalkar. *Foundations of machine learning*. MIT press, 2018.

- [31] Jishnu Mukhoti, Viveka Kulharia, Amartya Sanyal, Stuart Golodetz, Philip Torr, and Puneet Dokania. Calibrating deep neural networks using focal loss. *Advances in Neural Information Processing Systems (NeurIPS)*, 2020.
- [32] Rafael Müller, Simon Kornblith, and Geoffrey E Hinton. When does label smoothing help? *Advances in Neural Information Processing Systems (NeurIPS)*, 2019.
- [33] Allan H. Murphy. Scalar and vector partitions of the probability score : Part i. two-state situation. *Journal of Applied Meteorology (1962-1982)*, 1972.
- [34] Mahdi Pakdaman Naeini, Gregory Cooper, and Milos Hauskrecht. Obtaining well calibrated probabilities using bayesian binning. In *AAAI Conference on Artificial Intelligence (AAAI)*, 2015.
- [35] Ryumei Nakada, Halil Ibrahim Gulluk, Zhun Deng, Wenlong Ji, James Zou, and Linjun Zhang. Understanding multimodal contrastive learning and incorporating unpaired data. In *International Conference on Artificial Intelligence and Statistics*, pages 4348–4380. PMLR, 2023.
- [36] Giung Nam, Byeongho Heo, and Juho Lee. Lipsum-ft: Robust fine-tuning of zero-shot models using random text guidance. *International Conference on Learning Representations (ICLR)*, 2024.
- [37] Changdae Oh, Junhyuk So, Yongtaek Lim, Hoyoon Byun, Minchul Shin, Jong-June Jeon, and Kyungwoo Song. Geodesic multi-modal mixup for robust fine-tuning. *Advances in Neural Information Processing Systems (NeurIPS)*, 2023.
- [38] Sangdon Park, Osbert Bastani, James Weimer, and Insup Lee. Calibrated prediction with covariate shift via unsupervised domain adaptation. In *International Conference on Artificial Intelligence and Statistics (AISTATS)*, 2020.
- [39] Hieu Pham, Zihang Dai, Golnaz Ghiasi, Kenji Kawaguchi, Hanxiao Liu, Adams Wei Yu, Jiahui Yu, Yi-Ting Chen, Minh-Thang Luong, Yonghui Wu, Mingxing Tan, and Quoc V. Le. Combined scaling for zero-shot transfer learning. *Neurocomputing*, 555:126658, 2023. ISSN 0925-2312. doi: <https://doi.org/10.1016/j.neucom.2023.126658>. URL <https://www.sciencedirect.com/science/article/pii/S0925231223007816>.
- [40] Alec Radford, Jong Wook Kim, Chris Hallacy, Aditya Ramesh, Gabriel Goh, Sandhini Agarwal, Girish Sastry, Amanda Askell, Pamela Mishkin, Jack Clark, et al. Learning transferable visual models from natural language supervision. In *International Conference on Machine Learning (ICML)*, 2021.
- [41] Alexandre Ramé, Kartik Ahuja, Jianyu Zhang, Matthieu Cord, Léon Bottou, and David Lopez-Paz. Model ratatouille: Recycling diverse models for out-of-distribution generalization. In *International Conference on Machine Learning (ICML)*, 2023.
- [42] Benjamin Recht, Rebecca Roelofs, Ludwig Schmidt, and Vaishal Shankar. Do imagenet classifiers generalize to imagenet? In *International Conference on Machine Learning (ICML)*, 2019.
- [43] Yangjun Ruan, Yann Dubois, and Chris J Maddison. Optimal representations for covariate shift. In *International Conference on Learning Representations*, 2022.
- [44] Frederick Sanders. On subjective probability forecasting. *Journal of Applied Meteorology (1962-1982)*, (2):191–201, 1963.
- [45] Murat Sensoy, Lance Kaplan, and Melih Kandemir. Evidential deep learning to quantify classification uncertainty. *Advances in Neural Information Processing Systems (NeurIPS)*, 2018.
- [46] Yang Shu, Xingzhuo Guo, Jialong Wu, Ximei Wang, Jianmin Wang, and Mingsheng Long. Clipood: Generalizing clip to out-of-distributions. In *International Conference on Machine Learning*, pages 31716–31731. PMLR, 2023.
- [47] Christian Szegedy, Vincent Vanhoucke, Sergey Ioffe, Jon Shlens, and Zbigniew Wojna. Rethinking the inception architecture for computer vision. In *IEEE Conference on Computer Vision and Pattern Recognition (CVPR)*, 2016.
- [48] Sunil Thulasidasan, Gopinath Chennupati, Jeff A Bilmes, Tanmoy Bhattacharya, and Sarah Michalak. On mixup training: Improved calibration and predictive uncertainty for deep neural networks. *Advances in Neural Information Processing Systems (NeurIPS)*, 2019.
- [49] Junjiao Tian, Zecheng He, Xiaoliang Dai, Chih-Yao Ma, Yen-Cheng Liu, and Zsolt Kira. Trainable projected gradient method for robust fine-tuning. In *IEEE Conference on Computer Vision and Pattern Recognition (CVPR)*, 2023.

- [50] Junjiao Tian, Yen-Cheng Liu, James Smith, and Zsolt Kira. Fast trainable projection for robust fine-tuning. In *Advances in Neural Information Processing Systems (NeurIPS)*, 2023.
- [51] Christian Tomani, Sebastian Gruber, Muhammed Ebrar Erdem, Daniel Cremers, and Florian Buettner. Post-hoc uncertainty calibration for domain drift scenarios. In *IEEE Conference on Computer Vision and Pattern Recognition (CVPR)*, 2021.
- [52] Haohan Wang, Songwei Ge, Zachary Lipton, and Eric P Xing. Learning robust global representations by penalizing local predictive power. In *Advances in Neural Information Processing Systems (NeurIPS)*, 2019.
- [53] Mitchell Wortsman, Gabriel Ilharco, Jong Wook Kim, Mike Li, Simon Kornblith, Rebecca Roelofs, Raphael Gontijo Lopes, Hannaneh Hajishirzi, Ali Farhadi, Hongseok Namkoong, et al. Robust fine-tuning of zero-shot models. In *IEEE Conference on Computer Vision and Pattern Recognition (CVPR)*, 2022.
- [54] Yaodong Yu, Stephen Bates, Yi Ma, and Michael Jordan. Robust calibration with multi-domain temperature scaling. *Advances in Neural Information Processing Systems (NeurIPS)*, 2022.
- [55] Li Yuan, Francis EH Tay, Guilin Li, Tao Wang, and Jiashi Feng. Revisiting knowledge distillation via label smoothing regularization. In *IEEE Conference on Computer Vision and Pattern Recognition (CVPR)*, 2020.
- [56] Bianca Zadrozny and Charles Elkan. Transforming classifier scores into accurate multiclass probability estimates. In *ACM SIGKDD International Conference on Knowledge Discovery and Data Mining (KDD)*, 2002.
- [57] Chang-Bin Zhang, Peng-Tao Jiang, Qibin Hou, Yunchao Wei, Qi Han, Zhen Li, and Ming-Ming Cheng. Delving deep into label smoothing. *IEEE Transactions on Image Processing*, 2021.
- [58] Hongyi Zhang, Moustapha Cisse, Yann N Dauphin, and David Lopez-Paz. mixup: Beyond empirical risk minimization. *arXiv preprint arXiv:1710.09412*, 2017.
- [59] Jize Zhang, Bhavya Kailkhura, and T Yong-Jin Han. Mix-n-match: Ensemble and compositional methods for uncertainty calibration in deep learning. In *International Conference on Machine Learning (ICML)*, 2020.
- [60] Qi Zhang, Yifei Wang, and Yisen Wang. On the generalization of multi-modal contrastive learning. In *International Conference on Machine Learning*, pages 41677–41693. PMLR, 2023.
- [61] Yifan Zhang, Bryan Hooi, Dapeng Hu, Jian Liang, and Jiashi Feng. Unleashing the power of contrastive self-supervised visual models via contrast-regularized fine-tuning. *Advances in Neural Information Processing Systems*, 34:29848–29860, 2021.
- [62] Zhilu Zhang and Mert Sabuncu. Self-distillation as instance-specific label smoothing. In *Advances in Neural Information Processing Systems (NeurIPS)*, 2020.
- [63] Han Zhao, Shanghang Zhang, Guanhang Wu, José M. F. Moura, Joao P Costeira, and Geoffrey J Gordon. Adversarial multiple source domain adaptation. In *Advances in Neural Information Processing Systems (NeurIPS)*, 2018.
- [64] Han Zhao, Remi Tachet Des Combes, Kun Zhang, and Geoffrey Gordon. On learning invariant representations for domain adaptation. In *International conference on machine learning*, pages 7523–7532. PMLR, 2019.

Appendix

A Experimental Detail

This section supplements §5 providing detailed explanations for experiments to enhance the reproducibility.

A.1 Details for numerical analysis on error bounds

In §5.1, we conducted toy experiments to perform empirical analyses that demonstrate our theoretical findings. We provide the details of the toy experiments using synthetic data.

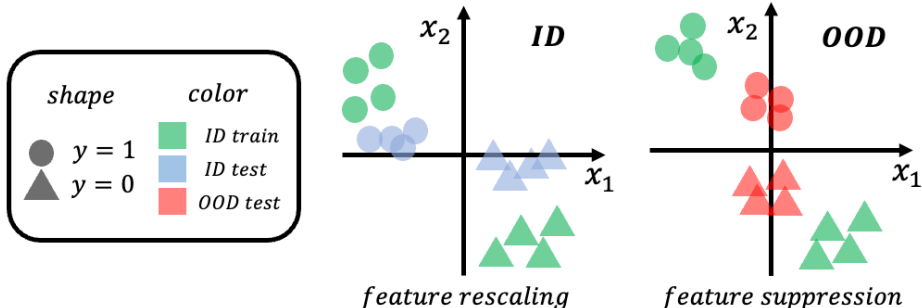


Figure A: Two-dimensional illustration of the experimental setup for numerical analyses. Note that the actual number of dimensions used for the experiments is set to 1000.

We generate 1000-dimensional Gaussian random variables, where the variables have binary noisy labels (15% of random flip) for the ID train, ID test, and OOD test datasets. For the ID train set, the first 400 dimensions and the second 400 dimensions are correlated with labels, and the remaining 200 dimensions are zero-centered random noises. We build the OOD test set from the ID test set by shifting the mean of the first 400 dimensions and downscaling the second 400 dimensions in half. The remaining 200 dimensions are intact. For example, the feature x_2 in Figure A is perfectly correlated with labels across train and test in both ID and OOD environments, while the correlation between feature x_1 and labels vanish in OOD environment. We train the three-layer multi-layer perceptron networks with four different learning objectives adopting regularization terms for calibration (\mathcal{L}_{SD}) and for the smallest singular value (\mathcal{L}_{OC}) with varying regularization magnitudes (111 models in total): (i) without regularization (Baseline) (ii) with \mathcal{L}_{SD} , (iii) with \mathcal{L}_{OC} , and (iv) with \mathcal{L}_{SD} and \mathcal{L}_{OC} . For \mathcal{L}_{OC} , we use an orthogonal constraint over the last weight matrix. For \mathcal{L}_{SD} , we adopt Born-Again-Network (BAN)-style self-distillation [10]. After training, we measured σ_{min} and ECE on the ID test set and measured the mean squared error (MSE) and ECE on OOD test set.

A.2 Benchmark datasets

This section supplements the summarized explanations of datasets provided in §5.2.

Training and test splits of ImageNet-1K [8] consist of 1000 classes, and its variants have the entire 1000 or a subset of the classes. Following Radford et al. [40] and Goyal et al. [13], we use the OpenAI templates to create text descriptions for each class (80 templates per class) for evaluation, and the averaged text representation is used as the final class representation for evaluation. Several related datasets including ImageNet-V2 [42], ImageNet-Rendition [18], ImageNet-A [19], ImageNet-Sketch [52], and ObjectNet [2] are employed to evaluate robustness of models. These datasets consist of similar semantic classes but are collected from different input distributions or styles.

A.3 Baseline methods

This section supplements the summarized explanations of baseline methods discussed in §5.2.

Zero-shot (ZS [40]): Zero-shot classifier is obtained by encoding and averaging text representations of each class using the pre-trained CLIP text encoder.

Standard fine-tuning (FT [53]): Linear classification head is initialized with text representation vectors for each class encoded by pre-trained CLIP text encoder. Image encoder and linear classifier parameters are fine-tuned for 10 epochs with a learning rate of $3e-5$.

LP-FT [25]: Randomly initialized linear classification head is first trained upon frozen image encoder for 5 epochs and then both image encoder and linear head parameters are updated for 5 epochs. For each phase, we use a learning rate of $1e-2$ and $3e-5$, respectively.

Fine-tuning with contrastive learning (FLYP [13]): Both image and text encoders are updated without additional linear classification heads. To create text representations of training samples, we use the OpenAI template similar to the evaluation data. Unlike for evaluation, we do not take an average of 80 different templates. Instead, we use 80 versions of text prompts for each class to build training pairs. The training pairs are randomly selected throughout the training steps. We fine-tune the model for 10 epochs (in total, 25K steps) with a learning rate of $1e-5$.

Lipsum-FT [36]: Cross-entropy loss with a regularization term that minimizes the energy gap between image and text is used as fine-tuning objective. We followed the details described in the original paper.

CaRot (Ours): We set the orthogonality constraint coefficient λ_{OC} as 0.2 and self-distillation coefficient λ_{SD} as 1.5, update frequency for EMA teacher as 500, and EMA final target momentum as 0.9. We linearly increased the EMA momentum α by 0.05 for the first 20% iterations. We followed all the other details from FLYP.

B Additional Evaluation Results

In addition to the comparisons of our CaRot with zero-shot, naive fine-tuning, and robust fine-tuning methods in §5.3, we provide results when applying post-hoc techniques for robustness (weight ensembling) and calibration (temperature scaling). Moreover, we compare our self-distillation-based soft label with uniform constant label smoothing.

B.1 Comparing approaches

Weight average of fine-tuned and zero-shot (WiSE-FT [53]): Zero-shot and fine-tuned model weights are averaged with a strength of ensembling coefficient. This ensembling technique can be applied to any fine-tuning method. We tune the ensembling coefficient for each method based on the ImageNet ECE value (we picked the value having the lowest ID ECE for each method).

Temperature scaling (TS [14]): Before applying the softmax function to compute output probability distribution, TS divides the logit by temperature $\tau \in (0, \infty)$. $\tau \rightarrow 0$ makes the probability similar to point masses (sharpening), $\tau \rightarrow \infty$ makes uniform distribution (smoothing). Scaling the output distribution does not affect accuracy since it does not change the model prediction (i.e., the probability rank remains the same). Temperature value was tuned for each method on the ID validation set based on the ECE value.

Label smoothing (LS [47]): LS is a regularization strategy that pursues the generalization of classification by utilizing soft labels, which are derived by adding uniform distribution to the hard label distribution. The soft label can be viewed as a new target probability distribution where the value of 1 to the target pair is reduced and the value of 0 for the non-target pair is increased by the smoothing parameter $\epsilon \in (0, 1)$. Since utilizing soft labels allows the model to pull negative pairs with limited strength, LS is beneficial for calibration beyond generalization by addressing the over-confidence issue [32].

B.2 Additional results

Results with WiSE are reported in Table A and B. We observe that weight ensembling, which aims to align zero-shot models and fine-tuned models in the model weight space, boosts the overall performance. Still, CaRot shows superior results to the baselines.

Results with TS can be found in Table C. Aligning with previous observations, applying TS significantly improves ID ECE. However, since TS adjusts the logits assuming that all data instances would have a similar extent of overconfidence (or underconfidence) issue, its positive effect is limited

under distribution shifts. Hence, TS does not guarantee to attain low calibration error on OOD datasets. It is noteworthy that applying TS even harms OOD ECE of CaRot (compare results with Table 3), which is already calibrated using data-dependent confidence adjustment during fine-tuning.

Results comparing with LS are reported in Table D. In accordance with its capability of improving calibration, LS successfully reduces calibration errors. We observe that our adopted approach, EMA SD, remarkably outperforms LS, especially on OOD ECE as well as in ID ECE. While LS addresses the over-confidence problem during train time by dispersing the concentrated confidence on the target label to non-target labels with a constant amount, self-distillation shows a similar behavior but in a dynamic approach, considering the diversity of data instances [62]. We interpret that reflecting the difficulty of input batch and distilling such information is crucial to achieving robust calibration.

We further provide an intuitive interpretation of self-distillation as an input-dependent approach to label smoothing as elaborated in Zhang and Sabuncu [62]. EMA SD provides soft labels considering the variation of data instances. For example, classifying a dog image from images of airplane or car could be less challenging than classifying it from images of cat or wolf. Ideally, a calibrated model should output higher confidence for the former case than for the latter. Instead of providing supervision of constantly adjusted confidence (as in LS), teacher predictions provide confidence reflecting the input data difficulty. Thereby, the student model can be supervised with high confidence diversity, which leads to a better-calibrated model. Please refer to Zhang and Sabuncu [62] for detailed discussions.

Table A: **Accuracy on ImageNet and distribution shifts using WiSE-FT [53]**. We select the optimal ensembling coefficient (i.e., α) for each method.

Method	IN \uparrow	IN-V2 \uparrow	IN-R \uparrow	IN-A \uparrow	IN-S \uparrow	ObjectNet \uparrow	Avg. shifts \uparrow
ZS	68.33	61.93	77.71	49.95	48.26	54.17	58.39
FT	81.96	72.69	77.19	51.93	53.17	56.83	62.36
LP-FT	82.63	73.14	75.24	51.92	51.99	55.86	61.63
FLYP	82.53	73.65	77.57	54.65	53.23	58.02	63.42
CaRot	82.36	73.72	79.58	54.07	53.96	57.70	63.81

Table B: **ImageNet ECE results with WiSE-FT [53]**. Along with Table A, we report the ECE results.

Method	IN \downarrow	IN-V2 \downarrow	IN-R \downarrow	IN-A \downarrow	IN-S \downarrow	ObjectNet \downarrow	Avg. shifts \downarrow
ZS	0.0570	0.0548	0.0541	0.0967	0.0850	0.0780	0.0736
FT	0.0714	0.0873	0.0744	0.1509	0.1391	0.1528	0.1209
LP-FT	0.0510	0.0895	0.0561	0.1917	0.1587	0.2014	0.1395
FLYP	0.0773	0.1087	0.0806	0.1963	0.1798	0.1995	0.1530
CaRot	0.0427	0.0416	0.0490	0.1207	0.0731	0.1113	0.0791

Table C: **ImageNet ECE results with temperature scaling (TS)**. Supplement to Table 2 and 3, we provide results applying TS. Note that TS is a post-hoc method and does not affect accuracy. The temperature is selected using IN ECE for each method.

Method	IN \downarrow	IN-V2 \downarrow	IN-R \downarrow	IN-A \downarrow	IN-S \downarrow	ObjectNet \downarrow	Avg. shifts \downarrow
ZS	0.0392	0.0633	0.0532	0.1792	0.1370	0.1760	0.1217
FT	0.0463	0.0786	0.0484	0.1798	0.1408	0.1820	0.1259
LP-FT	0.0382	0.0509	0.0477	0.1450	0.1028	0.1433	0.0979
FLYP	0.0392	0.0633	0.0532	0.1792	0.1370	0.1760	0.1217
Lipsum-FT	0.0380	0.0599	0.0419	0.1445	0.1165	0.1362	0.0998
CaRot	0.0401	0.0527	0.0437	0.1520	0.0802	0.1373	0.0931

B.3 Detailed results from main paper

Coefficient terms ablation. In Table F and E, we present the detailed ablation results of hyper-parameters associated with the methodologies addressed in our paper. These results supplement Table 5.

Table D: **Comparison on LS and EMA SD.** We compare the impact of LS and EMA SD with $\mathcal{L}_{\text{MCL-con}}$ as calibration regularization.

Method	Acc.↑						Avg. shifts
	IN	IN-V2	IN-R	IN-A	IN-S	ObjectNet	
-	82.51	73.18	71.80	48.16	49.78	54.67	59.51
LS	82.53	73.33	71.90	48.33	49.46	54.99	59.60
EMA SD	83.13	74.11	77.71	51.60	52.71	56.60	62.55
Method	ECE↓						Avg. shifts
	IN	IN-V2	IN-R	IN-A	IN-S	ObjectNet	
-	0.0651	0.1104	0.0910	0.2459	0.2132	0.2411	0.1803
LS	0.0475	0.0726	0.0526	0.1534	0.1533	0.1993	0.1262
EMA SD	0.0470	0.0367	0.0575	0.1240	0.0699	0.1075	0.0791

Table E: **Orthogonality constraint hyperparameter.** We report the impact of the orthogonality constraint term of CaRot objective by ablating its strength coefficient λ_{oc} . We set our final value as 0.2, tuning based on ID ECE.

λ_{oc}	Acc.↑						Avg. shifts
	IN	IN-V2	IN-R	IN-A	IN-S	ObjectNet	
0.1	83.18	74.10	77.53	51.35	52.66	56.47	62.42
0.2	83.13	74.11	77.71	51.60	52.71	56.60	62.55
0.5	83.04	74.40	77.64	51.04	52.63	56.49	62.44
1.0	83.09	74.35	77.59	51.23	52.65	56.62	62.49
λ_{oc}	ECE↓						Avg. shifts
	IN	IN-V2	IN-R	IN-A	IN-S	ObjectNet	
0.1	0.0511	0.0382	0.0620	0.1190	0.0712	0.0990	0.0779
0.2	0.0470	0.0367	0.0575	0.1240	0.0699	0.1075	0.0791
0.5	0.0478	0.0408	0.0579	0.1253	0.0701	0.1048	0.0798
1.0	0.0499	0.0380	0.0609	0.1201	0.0693	0.1022	0.0781

Table F: **Self-distillation term hyperparameter.** We report the impact of the EMA SD term of CaRot objective by ablating its strength coefficient λ_{SD} . We set our final value as 1.5, tuning based on σ_{min} .

λ_{SD}	Acc.↑						Avg. shifts
	IN	IN-V2	IN-R	IN-A	IN-S	ObjectNet	
0.5	83.07	74.22	74.37	50.76	51.49	56.08	61.38
1.0	83.23	74.51	76.38	51.05	52.47	56.63	62.21
1.5	83.03	74.13	77.59	50.72	52.49	56.49	62.28
2.0	82.72	74.14	78.25	50.71	53.13	56.49	62.54
λ_{SD}	ECE↓						Avg. shifts
	IN	IN-V2	IN-R	IN-A	IN-S	ObjectNet	
0.5	0.0482	0.0791	0.0599	0.2002	0.1533	0.1960	0.1377
1.0	0.0388	0.0544	0.0405	0.1640	0.0914	0.1481	0.0997
1.5	0.0523	0.0401	0.0642	0.1173	0.0732	0.0910	0.0772
2.0	0.0634	0.0467	0.0785	0.1030	0.0796	0.0829	0.0781

Different VLM backbones. We provide the full results of Table 7 in Table G and H.

Visualization of ECE values. Figure B illustrates the reliability diagram of ImageNet ECE results reported in Table 3.

Table G: ImageNet results on CLIP ResNet50

Method	Acc.↑					ObjectNet	Avg. shifts
	IN	IN-V2	IN-R	IN-A	IN-S		
ZS	59.83	52.90	60.72	23.25	35.45	40.27	42.52
FT	76.21	64.87	50.66	18.11	33.90	42.32	41.97
LP-FT	76.25	64.48	49.55	18.60	33.33	42.13	41.62
FLYP	76.16	65.10	51.55	20.08	34.24	42.53	42.70
CaRot (Ours)	76.12	65.36	52.16	19.32	34.05	42.67	42.71
ECE↓							
ZS	0.0624	0.0559	0.0530	0.2048	0.0740	0.0899	0.0955
FT	0.0983	0.1623	0.1860	0.4692	0.2824	0.3023	0.2804
LP-FT	0.1042	0.1759	0.2709	0.5184	0.3520	0.3197	0.3274
FLYP	0.0516	0.0872	0.1439	0.3872	0.2021	0.2432	0.2127
CaRot (Ours)	0.0471	0.0601	0.0948	0.3435	0.3435	0.2127	0.1714

Table H: ImageNet results on CLIP ViT-L/14

Method	Acc.↑					ObjectNet	Avg. shifts
	IN	IN-V2	IN-R	IN-A	IN-S		
ZS	75.55	69.85	87.85	70.76	59.61	66.59	70.93
FT	84.74	75.32	75.36	55.65	54.44	59.76	64.11
LP-FT	85.26	76.76	80.21	55.95	56.84	60.12	65.98
FLYP	86.19	78.21	83.81	68.85	60.20	66.15	71.44
CaRot (Ours)	86.95	79.28	87.96	72.68	62.66	68.05	74.13
ECE↓							
ZS	0.0590	0.0686	0.0339	0.0640	0.1037	0.0852	0.0711
FT	0.1056	0.1741	0.1613	0.3151	0.3234	0.2865	0.2521
LP-FT	0.0993	0.1531	0.0872	0.2593	0.2613	0.2572	0.2036
FLYP	0.0729	0.1219	0.0621	0.1443	0.2164	0.1903	0.1470
CaRot (Ours)	0.0349	0.0634	0.0353	0.0732	0.0914	0.1051	0.0737

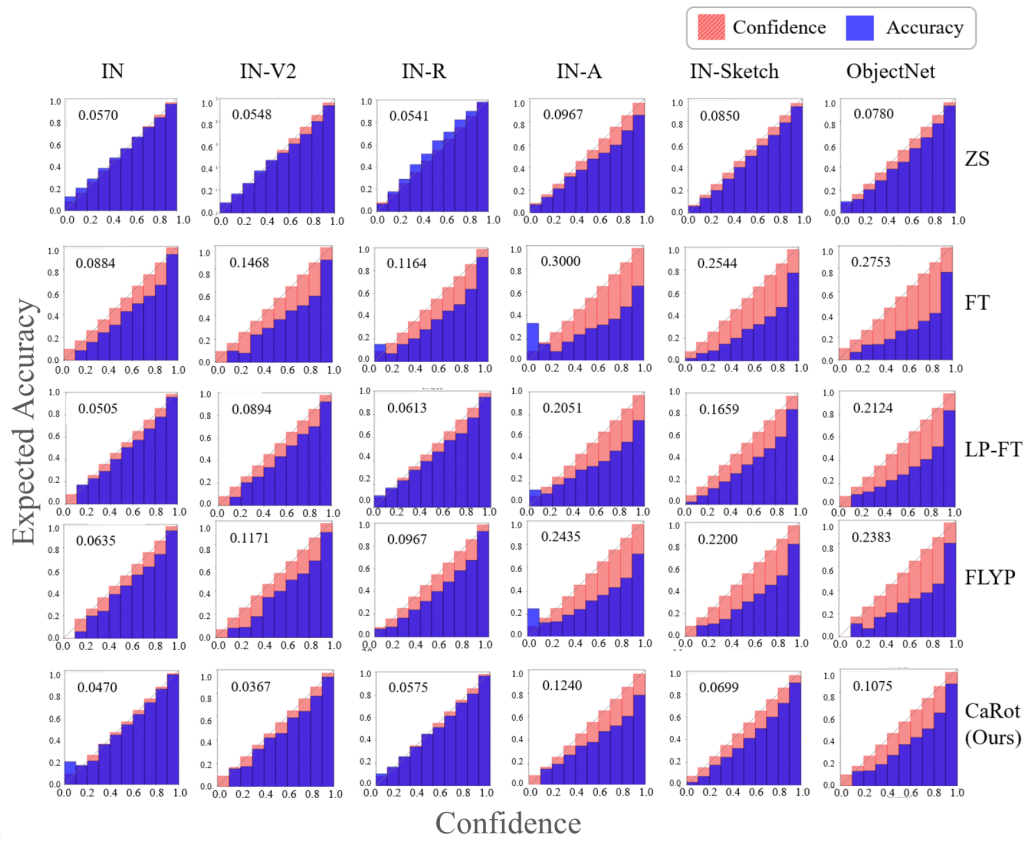


Figure B: **Reliability diagram of ImageNet ECE.** This figure supplements ECE results in Table 3. The value inside each plot indicates ECE.

C Proof

In this section, we provide a proof for Theorem 3.

Theorem C.1 (Restatement of Theorem 3.). *Let $h : \mathcal{X} \rightarrow [0, 1]$ be a real-valued function which has structure $h(x) = \sum_{i=1}^d h_i(x_i)$ where h_i is an arbitrary one-dimensional function, and $h(\cdot)$ is in a hypothesis class \mathcal{H} that has pseudo dimension $\mathcal{Pdim}(\mathcal{H}) = d_h$, $\hat{\mathcal{D}}_{ID}$ be an N -size empirical distribution on ID domain. If (x_i, x_j) is a bi-variate Gaussian random variable for every $i, j \in [d]$, then for any $\delta \in (0, 1)$ and for all h , the following bounds hold with probability at least $1 - \delta$:*

$$i) \quad \varepsilon_{\mathcal{D}_{OOD}}(h) \leq \varepsilon_{\hat{\mathcal{D}}_{ID}}(h) + \frac{d}{\sigma_{\min}(\tilde{\Sigma}_{\mathcal{D}_{ID}})} + \Delta + \mathcal{O}\left(\sqrt{\frac{1}{N} \log\left(\frac{N}{d_h}\right) \left(\frac{1}{\delta}\right)^{d_h}}\right), \quad (6)$$

$$ii) \quad \mathbb{E}_{\mathcal{D}_{OOD}}[(h(x) - y)^2] + \mathbb{E}_{\mathcal{D}_{OOD}}[c(x)^2] - 1 \leq \varepsilon_{\hat{\mathcal{D}}_{ID}}(h) + \frac{d}{\sigma_{\min}(\tilde{\Sigma}_{\mathcal{D}_{ID}})} + \Delta + \mathcal{O}\left(\sqrt{\frac{1}{N} \log\left(\frac{N}{d_h}\right) \left(\frac{1}{\delta}\right)^{d_h}}\right), \quad (7)$$

where $\tilde{\Sigma}_{\mathcal{D}_{ID}} := \mathbb{E}_{\mathcal{D}_{ID}}[\tilde{x}\tilde{x}^T]$ is a covariance matrix of d -dimensional normalized input $\tilde{x} = (\tilde{x}_1, \dots, \tilde{x}_d)$, where $\tilde{x}_i := (x_i - \mathbb{E}[x_i])\text{Var}(x_i)^{-1/2}$ and $\sigma_{\min}(M)$ is the smallest singular value of a matrix $M \in \mathbb{R}^{d_1 \times d_2}$.

Proof. The proof for the above theorem is divided into three steps: 1) the derivation of OOD calibration error bound, 2) the derivation of OOD generalization bound, and 3) the replacement of domain discrepancy term over ID and OOD into an ID-depend singular value term.

We first define a domain discrepancy measure \mathcal{H} -square disagreement, $sd_{\mathcal{H}}$, between two distributions as below:

Definition C.2 (\mathcal{H} -square disagreement). *Given two probability distributions \mathcal{D}_{OOD} and \mathcal{D}_{ID} over input space \mathcal{X} , \mathcal{H} as a hypothesis class containing the hypothesis $h(\cdot) : \mathcal{X} \rightarrow [0, 1]$, the discrepancy between \mathcal{D}_{OOD} and \mathcal{D}_{ID} is defined as*

$$sd_{\mathcal{H}}(\mathcal{D}_{OOD}, \mathcal{D}_{ID}) := \sup_{h, h' \in \mathcal{H}} |\mathbb{E}_{\mathcal{D}_{OOD}}[(h(x) - h'(x))^2] - \mathbb{E}_{\mathcal{D}_{ID}}[(h(x) - h'(x))^2]|. \quad (8)$$

The \mathcal{H} -square disagreement can be regarded as a variant of H-divergence [4] which adopts mean square error term rather than 0 – 1 classification loss or mean absolute error term as in [63].

Proposition C.3 (OOD calibration error bound). *Let $h : \mathcal{X} \rightarrow [0, 1]$ be a real-valued function in a hypothesis class \mathcal{H} with a pseudo dimension $\mathcal{Pdim}(\mathcal{H}) = d_h$. If $\hat{\mathcal{D}}_{ID}$ is an empirical distribution constructed by N -size i.i.d. samples drawn from \mathcal{D}_{ID} , then for any $\delta \in (0, 1)$, and for all h , a bound below hold with probability at least $1 - \delta$.*

$$\varepsilon_{\mathcal{D}_{OOD}}(h) \leq \varepsilon_{\hat{\mathcal{D}}_{ID}}(h) + sd_{\mathcal{H}}(\mathcal{D}_{OOD}, \mathcal{D}_{ID}) + \Delta + \mathcal{O}\left(\sqrt{\frac{1}{N} \left(\log \frac{1}{\delta} + d_h \log \frac{N}{d_h}\right)}\right). \quad (9)$$

Now, likewise Lemma 3 of [63], we start to review a triangle inequality for all $h, h', h'' \in \mathcal{H}$, for any \mathcal{D} on \mathcal{X} , and for error function $\varepsilon_{\mathcal{D}}(\cdot, \cdot)$, the inequality $\varepsilon_{\mathcal{D}}(h, h') \leq \varepsilon_{\mathcal{D}}(h, h'') + \varepsilon_{\mathcal{D}}(h'', h')$ holds. Here, we use $\varepsilon_{\mathcal{D}}(h, h')$ to denote $\mathbb{E}_{x \sim \mathcal{D}}[(h(x) - h'(x))^2]$. Now, given $h^* := \arg \min_{h \in \mathcal{H}} \varepsilon_{\mathcal{D}_{ID}}(h) + \varepsilon_{\mathcal{D}_{OOD}}(h)$ and $\Delta := \varepsilon_{\mathcal{D}_{ID}}(h^*) + \varepsilon_{\mathcal{D}_{OOD}}(h^*)$, we have

$$\begin{aligned} \varepsilon_{\mathcal{D}_{OOD}}(h) &\leq \varepsilon_{\mathcal{D}_{OOD}}(h^*) + \varepsilon_{\mathcal{D}_{OOD}}(h, h^*) \\ &= \varepsilon_{\mathcal{D}_{OOD}}(h^*) + \varepsilon_{\mathcal{D}_{OOD}}(h, h^*) - \varepsilon_{\mathcal{D}_{ID}}(h, h^*) + \varepsilon_{\mathcal{D}_{ID}}(h, h^*) \\ &\leq \varepsilon_{\mathcal{D}_{OOD}}(h^*) + |\varepsilon_{\mathcal{D}_{OOD}}(h, h^*) - \varepsilon_{\mathcal{D}_{ID}}(h, h^*)| + \varepsilon_{\mathcal{D}_{ID}}(h, h^*) \\ &\leq \varepsilon_{\mathcal{D}_{OOD}}(h^*) + \varepsilon_{\mathcal{D}_{ID}}(h, h^*) + sd_{\mathcal{H}}(\mathcal{D}_{OOD}, \mathcal{D}_{ID}) \\ &\leq \varepsilon_{\mathcal{D}_{OOD}}(h^*) + \varepsilon_{\mathcal{D}_{ID}}(h) + \varepsilon_{\mathcal{D}_{ID}}(h^*) + sd_{\mathcal{H}}(\mathcal{D}_{OOD}, \mathcal{D}_{ID}) \\ &= \varepsilon_{\mathcal{D}_{ID}}(h) + sd_{\mathcal{H}}(\mathcal{D}_{OOD}, \mathcal{D}_{ID}) + \Delta. \end{aligned} \quad (10)$$

where $\varepsilon_{\mathcal{D}}(h)$ is defined as $\varepsilon_{\mathcal{D}}(h) := \mathbb{E}_{x \sim \mathcal{D}}[(h(x) - h_0(x))^2]$ and $h_0(\cdot) := \arg \min_{h \in \mathcal{H}} \mathbb{E}_x[(h(x) - c(x))^2]$ denotes a desired calibrated predictor of label y when $c(x) := \mathbb{E}_{\mathcal{D}}[y|h(x)]$. Here, the first and fourth inequalities in Eq (10) are held by triangular inequality.

The above bound is defined over the true population distribution \mathcal{D}_{ID} and \mathcal{D}_{OOD} . For the ID domain, we can confine our analysis to empirical distribution $\hat{\mathcal{D}}_{\text{ID}}$ with N i.i.d. samples generated from \mathcal{D}_{ID} , by leveraging a generalization bound on a single domain regression setting [30, 63]. If $\mathcal{P}dim(\mathcal{H}) = d_h$, for all $h \in \mathcal{H}$, below bound holds with probability at least $1 - \delta$ (See Lemma 5 of Zhao et al. [63]).

$$\varepsilon_{\mathcal{D}_{\text{OOD}}}(h) \leq \varepsilon_{\hat{\mathcal{D}}_{\text{ID}}}(h) + sd_{\mathcal{H}}(\mathcal{D}_{\text{OOD}}, \mathcal{D}_{\text{ID}}) + \Delta + \mathcal{O}\left(\sqrt{\frac{1}{N} \left(\log \frac{1}{\delta} + d_h \log \frac{N}{d_h}\right)}\right). \quad (11)$$

The above bound is similar to a regression bound proposed by Zhao et al. [63], but we build the theory based on the squared error rather than the previously adopted absolute error. This slight change allows us two attractive extensions that we will introduce to achieve calibrated robust fine-tuning.

While Proposition C.3 provides guidance to pursue OOD calibration, it does not say anything about OOD classification error, which is our primary goal before calibration. Here, we pay attention to the decomposition of the Brier score [33, 38]:

$$\underbrace{\mathbb{E}[(h(x) - y)^2]}_{\text{classification error}} = \underbrace{\mathbb{E}[(h(x) - c(x))^2]}_{\text{calibration error}} + 1 - \underbrace{\mathbb{E}[c(x)^2]}_{\text{sharpness}}, \quad (12)$$

where $\mathbb{E}[(h(x) - y)^2]$ is an expected mean-squared classification error and $\mathbb{E}[c(x)^2]$ denotes the sharpness [44] term rewarding the predictor $h(\cdot)$ to produce outputs towards zero or one. By assuming that $h(\cdot)$ is expressive enough to estimate the ground truth expectation function for the label, i.e., $c(\cdot)$, plugging Eq. (12) into the LHS of Proposition C.3 derives the same (except a constant) upper bound for the sum of classification error and prediction sharpness on OOD samples as in Proposition C.4.

Proposition C.4 (OOD generalization error bound). *Let $h(\cdot)$, \mathcal{H} , and $\hat{\mathcal{D}}_{\text{ID}}$ have the same definition as in Proposition C.3, then for any $\delta \in (0, 1)$, and for all h , a bound hold with prob. at least $1 - \delta$,*

$$\mathbb{E}_{\mathcal{D}_{\text{OOD}}}[(h(x) - y)^2] + \mathbb{E}_{\mathcal{D}_{\text{OOD}}}[c(x)^2] - 1 \leq \varepsilon_{\hat{\mathcal{D}}_{\text{ID}}}(h) + sd_{\mathcal{H}}(\mathcal{D}_{\text{OOD}}, \mathcal{D}_{\text{ID}}) + \Delta + \mathcal{O}\left(\sqrt{\frac{1}{N} \left(\log \frac{1}{\delta} + d_h \log \frac{N}{d_h}\right)}\right). \quad (13)$$

From domain discrepancy to minimum singular value. The second term $sd_{\mathcal{H}}(\mathcal{D}_{\text{OOD}}, \mathcal{D}_{\text{ID}})$ of RHS of Proposition C.3 and Proposition C.4 is defined on both ID and OOD samples, so it is hard to control the quantity directly. While existing approaches attempt to learn domain-invariant representations for reducing the similar quantity (e.g., H-divergence) by using unlabeled OOD data [11, 63, 64], the OOD data are commonly inaccessible on many real-world applications. Therefore, we need a quantity that is solely defined with ID data. Recently, Dong and Ma [9] proved that the domain discrepancy ratio can be bounded from above by a reciprocal of the smallest singular value of a covariance matrix of ID data as below:

$$\sup_{h, h' \in \mathcal{H}} \frac{\mathbb{E}_{\mathcal{D}_{\text{OOD}}}(h(x) - h'(x))^2}{\mathbb{E}_{\mathcal{D}_{\text{ID}}}(h(x) - h'(x))^2} \leq \frac{d}{\sigma_{\min}(\tilde{\Sigma}_{\mathcal{D}_{\text{ID}}})}, \quad (14)$$

where $\tilde{\Sigma}_{\mathcal{D}_{\text{ID}}} := \mathbb{E}_{\mathcal{D}_{\text{ID}}}[\tilde{x}\tilde{x}^T]$ is a covariance matrix of the d -dimensional normalized input $\tilde{x} = (\tilde{x}_1, \dots, \tilde{x}_d)$ where $\tilde{x}_i := (x_i - \mathbb{E}[x_i])\text{Var}(x_i)^{-1/2}$ and $\sigma_{\min}(M)$ is the minimum singular value of a matrix $M \in \mathbb{R}^{d_1 \times d_2}$.

Lemma C.5. *Assuming that OOD calibration error is always greater than the ID calibration error and noting that the range of $h(\cdot)$ is $[0, 1]$, the second term $sd_{\mathcal{H}}(\mathcal{D}_{\text{OOD}}, \mathcal{D}_{\text{ID}})$ of RHS in Proposition C.3 and C.4 is bound from above by the smallest singular value of the normalized input covariance matrix. That is,*

$$sd_{\mathcal{H}}(\mathcal{D}_{\text{OOD}}, \mathcal{D}_{\text{ID}}) \leq \frac{d}{\sigma_{\min}(\tilde{\Sigma}_{\mathcal{D}_{\text{ID}}})}. \quad (15)$$

This can be easily shown by the definition of $sd_{\mathcal{H}}(\mathcal{D}_{\text{OOD}}, \mathcal{D}_{\text{ID}})$,

$$sd_{\mathcal{H}}(\mathcal{D}_{\text{OOD}}, \mathcal{D}_{\text{ID}}) = \sup_{h, h' \in \mathcal{H}} |\mathbb{E}_{\mathcal{D}_{\text{OOD}}}[(h(x) - h'(x))^2] - \mathbb{E}_{\mathcal{D}_{\text{ID}}}[(h(x) - h'(x))^2]| \quad (16)$$

$$\leq \sup_{h, h' \in \mathcal{H}} \frac{\mathbb{E}_{\mathcal{D}_{\text{OOD}}}(h(x) - h'(x))^2}{\mathbb{E}_{\mathcal{D}_{\text{ID}}}(h(x) - h'(x))^2} \quad (17)$$

$$\leq \frac{d}{\sigma_{\min}(\tilde{\Sigma}_{\mathcal{D}_{\text{ID}}})}. \quad (18)$$

Where the first inequality is held by the assumption of the Lemma C.5 and the second inequality is held by Theorem 3 of [9].

Finally, we can derive a more tractable bound for OOD classification and calibration error by plugging the Lemma C.5 into the Proposition C.3 and Proposition C.4.

□